

On the Universality of Energy Extraction from Black Hole Spacetimes

Koushik Chatterjee,^{1,2,*} Ziri Younsi,^{3,†} Prashant Kocherlakota,^{1,2,‡} and Ramesh Narayan^{2,1,§}

¹*Black Hole Initiative at Harvard University, 20 Garden St., Cambridge, MA 02138, USA*

²*Center for Astrophysics, Harvard & Smithsonian, 60 Garden St., Cambridge, MA 02138, USA*

³*Mullard Space Science Laboratory, University College London, Holmbury St. Mary, Dorking, Surrey, RH5 6NT*

(Dated: November 1, 2023)

The launching of astrophysical jets provides the most compelling observational evidence for direct extraction of black hole (BH) spin energy via the Blandford-Znajek (BZ) mechanism. Whilst it is known that spinning Kerr BHs within general relativity (GR) follow the BZ jet power relation, the nature of BH energy extraction in general theories of gravity has not been adequately addressed. This study performs the first comprehensive investigation of the BZ jet power relation by utilising a generalised BH spacetime geometry which describes parametric deviations from the Kerr metric of GR, yet recovers the Kerr metric in the limit that all deviation parameters vanish. Through performing and analysing an extensive suite of three-dimensional covariant magnetohydrodynamics (MHD) simulations of magnetised gas accretion onto these generalised BH spacetimes we find that the BZ jet power relation still holds, in some instances yielding jet powers far in excess of what can be produced by even extremal Kerr BHs. It is shown that the variation of the quadrupole moment of the BH can enhance or suppress the effects of BH spin, and by extension of frame-dragging. This variation greatly enhances or suppresses the observed jet power and underlying photon ring image asymmetry, introducing a previously unexplored yet important degeneracy in BH parameter inference.

I. INTRODUCTION

Astrophysical jets are an ubiquitous phenomenon in our Universe. From stellar-mass to supermassive black hole (BH) scales, relativistic outflows of plasma are observed to emanate from regions a few gravitational radii away from the central compact object and extend in excess of several millions to even several billions of gravitational radii, traversing galactic scales. As jets propagate outwards, they interact with and heat up the surrounding interstellar medium gas by depositing their magnetic and kinetic energy, seeding large-scale turbulent eddies [1–3]. Due to their ability to traverse and remain collimated across such large distances at relativistic velocities, astrophysical jets effectively act as energy conduits, transferring their kinetic (and potentially magnetic) energy to the interstellar medium. They are therefore major contributors to the AGN feedback cycle and their energy extraction and deposition mechanisms regulate star formation and galactic evolution [4–7].

The mechanism considered most likely to govern the launching of powerful jets is the Blandford-Znajek (BZ) mechanism [8]. Broadly speaking, within the BZ mechanism framework, the BH forces the magnetic field to co-rotate with the spin direction via the frame-dragging effect, twisting the field lines in the azimuthal direction. This twisting of magnetic field lines produces an outward magnetic pressure that eventually launches the jet. Since the twisting of field lines by frame-dragging can be thought of “work” done by the BH, there is an effective extraction of the BH’s rotational energy. Hence, the jet power output (P_{BZ}) via the BZ mechanism is directly related to the strength of the normalised magnetic flux (ϕ_{H}) at

the event horizon radius (r_{H}), and the BH spin (a). The BZ jet efficiency can be expressed more generally as:

$$\eta_{\text{BZ}} = \frac{P_{\text{BZ}}}{Mc^2} = \frac{k}{4\pi} \phi_{\text{H}}^2 \Omega_{\text{H}}^2, \quad (1)$$

where the horizon angular frequency $\Omega_{\text{H}} := ac/(2r_{\text{H}})$ for Kerr BHs [8–10]. The constant k depends on the parabolicity of the poloidal magnetic field ($k = 0.054$ for near-monopolar or purely radial magnetic fields and 0.044 for parabolic fields). Hereafter, we assume natural units $G = c = 1$ for our calculations, with the characteristic length- and time-scales given by the BH mass M .

General-relativistic magnetohydrodynamics (GRMHD) simulations have been instrumental in shaping our understanding of BH accretion physics, steadily growing in popularity due to their ability to describe the spatio-temporal evolution of the complex gas and magnetic field dynamics for a wide variety of accreting systems. In this work, we begin with a hydrodynamic torus of weakly magnetised gas, and then introduce a perturbation in the gas properties to trigger disk instabilities and finally, accretion onto the central BH. As time evolves, three distinct regions develop: a dense equatorial accretion flow with turbulent magnetic fields, a gas-rich, slow-moving wind outflowing from the disk and a near-vacuum, relativistic jet in the direction of the BH spin axis. Of these three structures, the jet is closest to the BZ solution that assumed force-free (or effectively, vacuum) electrodynamics. Thus, we expect that BHs where the jet dominates the total power output should, in principle, match the BZ expectation.

In the limit of a saturated BH magnetosphere, the accretion flow transitions to a magnetically arrested (MAD) state. MADs with highly spinning BHs have distinctive properties such as highly efficient jets with $\eta \gtrsim 1$, powerful enough to spindown of the BH [11–13]. MADs also exhibit quasi-periodic magnetic explosions that are thought to be the origin of high-energy flares and even gamma-rays [14]. The presence of strong vertical magnetic fields near the BH event horizon in

* koushik.chatterjee@cfa.harvard.edu

† z.younsi@ucl.ac.uk

‡ prashant.kocherlakota@cfa.harvard.edu

§ rnarayan@cfa.harvard.edu

MADs also makes them a favourable candidate for explaining the resolved polarisation structure of M87* [15]. As MADs describe the theoretical upper limit for the horizon magnetic flux, they are arguably the best candidates for investigating energy extraction from BHs via the BZ mechanism. Thus we opt for standard MAD initial conditions in this study [13, 16, 17].

II. THE JOHANSEN-PSALTIS METRIC

In order to explore deviations from the Kerr metric and GR, we consider the Johannsen-Psaltis (JP) metric [18–20]. The JP metric describes the exterior solution of a rapidly spinning BH and introduces parametric deviations to the Kerr metric via adjustable dimensionless deviation parameters. At lowest order there are four such parameters: ϵ_3 , α_{13} , α_{22} , α_{52} , of which we always set $\alpha_{52} = 0$ since this parameter affects only the g_{rr} metric component and does not alter the angular frequency or the innermost stable circular orbit (ISCO) of particles, nor the unstable photon orbit radius and therefore the observed photon ring image. The geodesic integrability and topological structure of the JP metric are well understood, enabling the study of rapidly spinning BHs that cannot be described by the Kerr solution, nor be admitted as a solution of the Einstein field equations of GR.

In this work we independently adjust the remaining three parameters: ϵ_3 only weakly alters the Kerr ISCO radius, α_{13} is $\mathcal{O}(r^{-3})$ and mildly alters the ISCO radius, and α_{22} is $\mathcal{O}(r^{-2})$ and significantly alters the ISCO radius. Regarding the photon ring radius, ϵ_3 has no effect, α_{13} alters its Kerr value and “circularises” the observed ring, and α_{22} also alters the ring radius but serves to enhance asymmetry. This latter point may be understood as α_{22} adjusting the quadrupole moment of the BH, thereby significantly enhancing the effects of frame-dragging beyond what is possible even for an extremal Kerr BH [21]. One therefore anticipates that large quadrupole moments (large values of α_{22}) will enhance energy extraction from the BH and yield much more powerful jets than even an extremal Kerr BH.

III. RESULTS

We perform a suite of 69 distinct 3D covariant MHD simulations including general relativity and parametric deviations from it with the JP metric. For brevity, we will refer to all simulations as “GRMHD”. Of these, 13 employ the Kerr metric, i.e., $a = (0, \pm 0.3, \pm 0.5, \pm 0.7, \pm 0.9, \pm 0.94, \pm 0.998)$, 19 simulations account for deviations solely in α_{13} , 27 simulations for deviations solely in α_{22} , and finally 10 simulations for deviations solely in ϵ_3 . Table I provides a summary of our simulation set. All of these simulations are evolved to $t = 25000M$ to make sure that the inner $30M$ are in inflow-outflow equilibrium. Here we only discuss quantities time-averaged between $20000M - 25000M$.

We focus on the calculation of the dimensionless magnetic flux on the BH event horizon ϕ_H and the outflow efficiency η_{out} , comprising the contributions of both the jet and disk

wind to outward energy transfer. The dimensionless magnetic flux is defined as:

$$\phi_H := \frac{\sqrt{4\pi}}{2\sqrt{M}} \iint |B^r| \sqrt{-g} d\theta d\varphi, \quad (2)$$

where the integral is calculated at the event horizon radius $r = r_H := M(1 + \sqrt{1 - a^2})$ (since the chosen JP parameters do not change the horizon size). In eqn. (2), B^r is the radial magnetic field component, g is the metric determinant, and \dot{M} is the shell-integrated mass accretion rate, $\dot{M}(r) = -\iint \rho u^r \sqrt{-g} d\theta d\varphi$, calculated at $r = 5M$ in order to avoid contamination from density floors. The outflow efficiency is given by:

$$\eta_{\text{out}} = \frac{P_{\text{out}}}{\dot{M}} = \frac{\dot{M} - \dot{E}}{\dot{M}}, \quad (3)$$

where P_{out} is the outflow power and $\dot{E} = \iint T_t^r \sqrt{-g} d\theta d\varphi$ the total energy flux in the radial direction, where the (r, t) component of the stress-energy tensor is expressed as $T_t^r = (\rho + \gamma_{\text{ad}} U_g + b^2) u^r u_t - b^r b_t$. Here, ρ represents the gas density, γ_{ad} its adiabatic index, U_g its internal energy, u^μ its four-velocity, and b^μ the magnetic four-vector. We calculate the outflow efficiency at $r = 5M$. Finally, the horizon angular frequency for the JP metric depends not only on the spin, but also on α_{13} and α_{22} in the following manner:

$$\Omega_H^{\text{JP}} = \frac{a}{2r_H} \frac{A_2(\alpha_{22}, r = r_H)}{A_1(\alpha_{13}, r = r_H)} = \Omega_H^{\text{Kerr}} \frac{A_2}{A_1} \Bigg|_{r=r_H}, \quad (4)$$

where $A_1 \equiv 1 + \alpha_{13}/r^3$ and $A_2 \equiv 1 + \alpha_{22}/r^2$. Thus, increasing α_{22} drives up the horizon angular frequency by enhancing frame-dragging while increasing α_{13} serves to suppress frame dragging, in effect decreasing Ω_H .

Using Eqn 1 and 4, we can compare the time-averaged total outflowing power efficiency η from our simulations with the corresponding expected BZ power (Fig. 1a). We find that outflow power follows the BZ formula for both Kerr and non-Kerr models, even at large values of $\Omega_H \phi_H$, i.e., when the jet dominates the total outflow. It is noteworthy that the maximal $|\Omega_H| = 1/2$ for Kerr BHs, whereas the non-zero quadrupole ($\alpha_{22} \neq 0$) models can reach larger horizon frequencies for the same BH spin.

Evidently, a degeneracy in η arises between BH spin and non-Kerr parameters. Panel (b) of Figure 1 shows that for a given spin, the range of possible outflow efficiencies for a non-Kerr BH is large, especially for larger values of a . Measuring the jet power may therefore not provide an accurate estimate of BH spin when the quadrupole moment α_{22} is of large and opposite sign, mimicking the effects of spin. Caution must therefore be exercised. For example, consider that for the highly spinning $a = 0.9$ BH, a value of $\alpha_{22} = -2$ results in a near-zero horizon frequency and barely produces an outflow, while $\alpha_{22} = 2$ exhibits $\eta \approx 330\%$, a factor of ≈ 2 larger than the Kerr $a = 0.998$ model.

To see the effect of introducing non-Kerr parameters on BH images, we performed general-relativistic radiative transfer (GRRT) calculations of a selection of GRMHD simulations

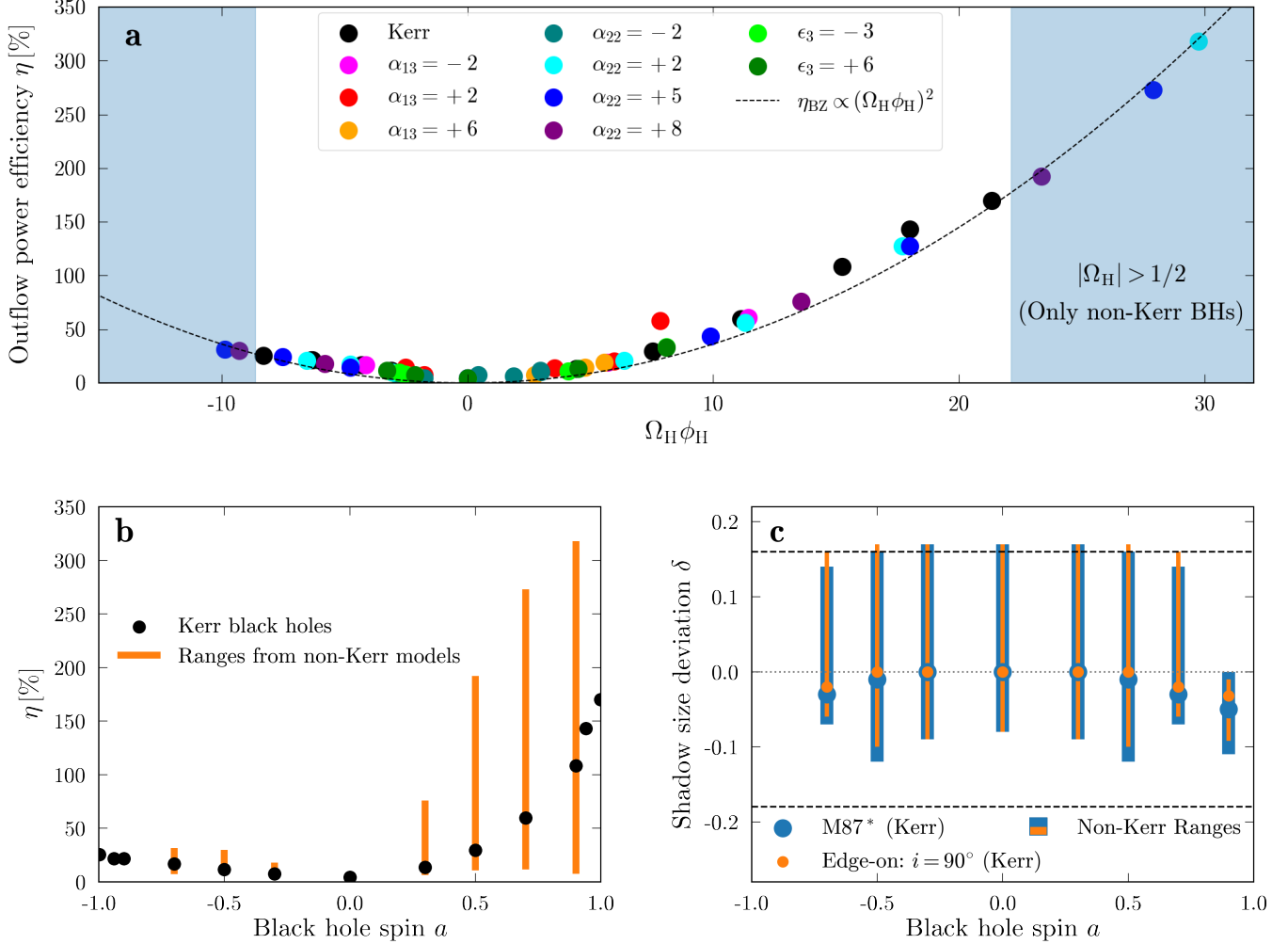


FIG. 1. Panel **a** demonstrates that the BZ mechanism accurately describes the outflow power for arbitrary non-Kerr BHs out to large horizon angular frequencies beyond even extremal Kerr BHs. This implies that the BZ power is a fundamental property of spinning BHs. Panel **b** shows that the outflow power can assume a large range of values given a particular BH spin within our model set. Panel **c** is similar to panel **b**, but now presents the deviation in mean BH shadow diameter with respect to the Schwarzschild value of $d_{\text{sh,Schw}} = 6\sqrt{3} M$, hereafter $\delta := d_{\text{sh}}/d_{\text{sh,Schw}} - 1$. We also show the 2017 EHT measurements of M87* of $\delta = -0.01 \pm 0.17$ [22–24], delineated as dashed lines. These plots illustrate the inherent degeneracies in BH spin inference from jet power estimates and shadow image size measurements when one relaxes the assumption that the spacetime geometry is described by a Kerr BH.

with the general-relativistic radiative transfer (GRRT) raytracing code BHOSS [25, 26], focusing on comparison with an $a = 0.5$ Kerr BH model. Figure 2 shows the 86 GHz and 230 GHz images for M87* parameters: a BH mass of $M_{\text{BH}} = 6.2 \times 10^9 M_\odot$ located at a distance of $D_{\text{BH}} = 16.9$ megaparsecs (around 55 million lightyears) viewed at a nearly face-on inclination of $i = 163^\circ$ [27]. More details about the GRRT methodology is given in the appendix.

The 86 GHz images for BH models with large outflow powers show more extended and distinctly collimated jets. Usually, non-thermal processes such as magnetic reconnection and shocks in jets [28] need to be invoked to reproduce large-scale extended jet images that are seen in astronomical observational, e.g., out to sizes $\gtrsim 500 \mu\text{as}$ for M87* [29]. We find that

we can reach such image sizes for moderate BH spins even without assuming non-thermal processes when we increase the quadrupole moment. Essentially, we can increase α_{22} to achieve a larger Ω_H , which in turn drives a more efficient and powerful jet, creating an extended image in a manner akin to how an increase in the BH spin leads to more extended jet images for Kerr BHs [29]. Since non-Kerr spacetimes permit $\Omega_H > 1/2$, jet images can be much more extended than is possible with even an extremal Kerr BH. On the other hand, we can also decrease Ω_H with the α_{13} parameter, resulting in a weakly powered jet that appears similar to the Schwarzschild 86 GHz jet image. Thus, as seen in η , the size of the 86 GHz image is intimately linked to the BH spacetime via the BZ process. Consequently, observing a large-scale jet does not

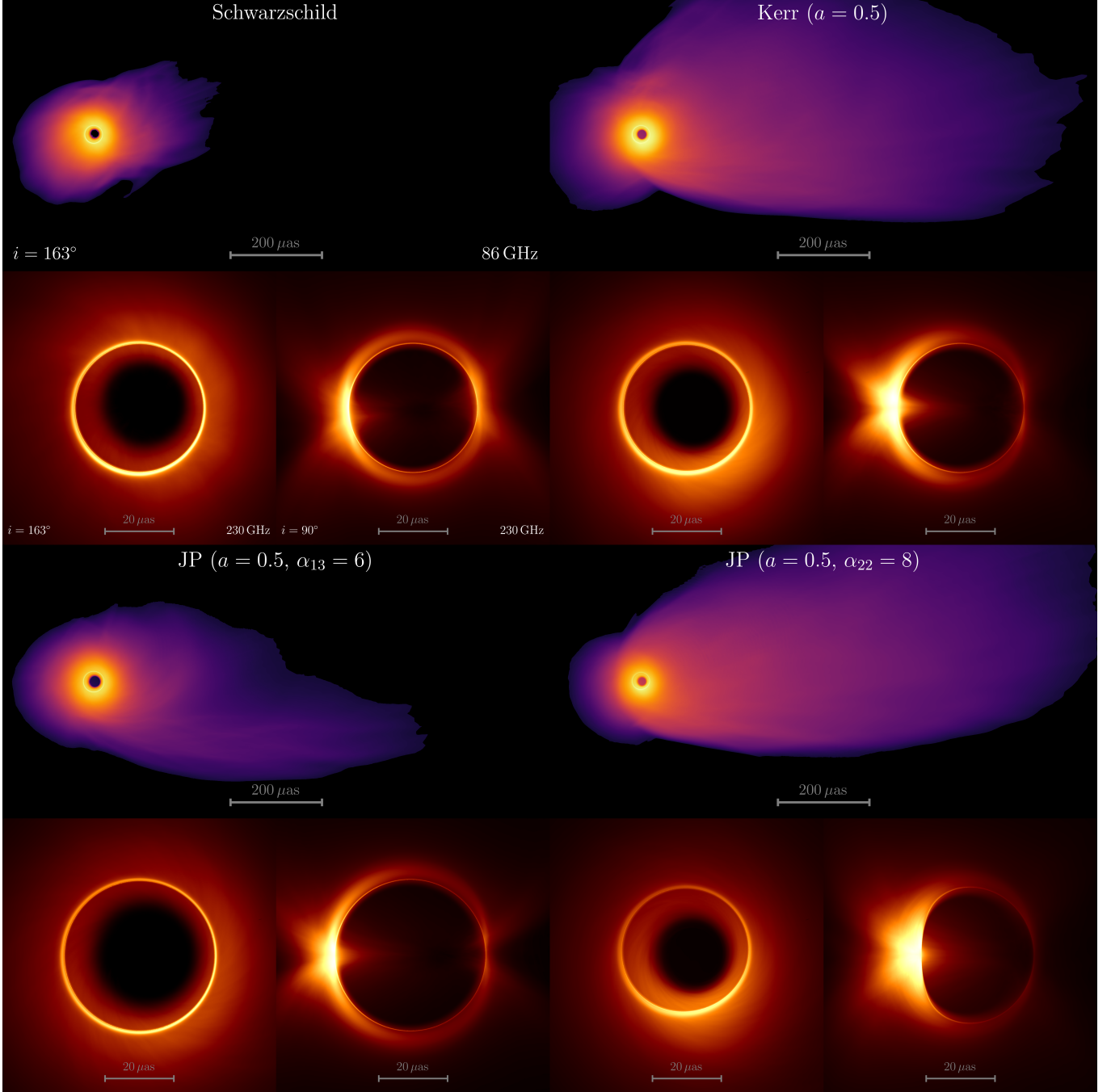


FIG. 2. Collection of three-image panel groups showing 86 GHz M87* images (upper panels) and corresponding 230 GHz BH shadow images (both viewed at $i = 163^\circ$, bottom left) and as viewed at $i = 90^\circ$ (bottom right). From left to right, top to bottom, trios of panels represent: Schwarzschild BH, Kerr BH with $a = 0.5$, JP BH with $\alpha_{13} = 6$ and $a = 0.5$, and a JP BH with $\alpha_{22} = 8$ and $a = 0.5$, respectively. Differences in jet size and power are evident between Schwarzschild and Kerr BHs at 86 GHz. The JP BH with $\alpha_{13} = 6$, in spite of having the same spin as the Kerr BH, has a significantly weaker jet and larger photon ring size. By contrast, the JP BH with $\alpha_{22} = 8$ possesses a strong quadrupole moment, enhancing the effects of frame dragging, giving rise to a more powerful and extended jet than the Kerr BH with identical spin. All panels show time-averaged images over the interval 20,000 M – 25,000 M. The 86 GHz image color scale is logarithmic and spans 5 orders of magnitude in specific intensity, whereas the 230 GHz images are plotted on a linear scale and show the full range of specific intensity. All images are normalised to a maximum pixel intensity of unity.

necessarily imply a rapidly spinning BH, as a small spin combined with a large quadrupole moment can enhance the spin and hence the amount of frame dragging, yielding a similar image to that produced by a more rapidly spinning Kerr BH.

One should also exercise caution when estimating spin from BH shadow size measurements. Panel (c) of figure 1 presents the theoretical mean shadow size calculations for Kerr BHs when viewed edge-on (i.e., an observer inclination angle $i = 90^\circ$) and at $i = 163^\circ$ (i.e., the inclination angle for M87*). The filled-in area indicates the range of shadow sizes allowed by our particular set of non-Kerr parameters for a given BH spin. We find that the variation in the shadow diameters is largest for a face-on observer whereas the asymmetry of the ring is largest for an edge-on observer, due to frame-dragging (see also Fig. 2). For the case of M87*, the observer is nearly face-on (163°) and the shadows are effectively circular. The BH models we use here all have similar shadow sizes.

Turning to the 230 GHz horizon-scale images, the image structure for M87* looks very similar between the models, as expected from panel (c) of Fig. 1. We also include the corresponding edge-on inclination cases to demonstrate the maximum deformation of the shadow shape and asymmetry of the image seen in Fig. 1c. In particular, as compared to the Kerr edge-on ($i = 90^\circ$) image, the corresponding shadow for $\alpha_{22} = 8$ shows a significant enhancement in prolateness and shifts towards the right, mimicking the effects of strong frame-dragging exhibited by rapidly spinning Kerr BHs. In fact, the horizon angular frequency of a JP BH with spin $a = 0.5$ and $\alpha_{22} = 8$ is similar to that of a Kerr BH with spin $a = 0.992$. Further, we see that the $\alpha_{13} = 6$ image looks remarkably similar to the Schwarzschild image since α_{13} acts to circularise the shadow image's shape, counteracting the effects of spin by reducing Ω_H , accompanied by a small increase in the shadow diameter. This reaffirms the large degeneracy in horizon-scale image morphologies between Kerr and non-Kerr BHs.

IV. DISCUSSION AND SUMMARY

In this paper, we verify that the BZ power efficiency $\eta_{BZ} \propto \phi_H^2 \Omega_H^2$ describes the outflow power for arbitrary spinning BH spacetimes. It is interesting to note that the BZ power formula has been extended to higher BH spins in orders of Ω_H^2 , out to $\mathcal{O}(\Omega_H^6)$ [10, 30], to preserve the non-dependence of the power output on BH spin direction for extremely high Kerr BH spins ($a \gtrsim 0.99$), in the form of $\eta_{BZ,ext} = \eta_{BZ} \times f(\Omega_H)$, where $f(\Omega_H) = 1 + 1.38 \Omega_H^2 - 9.2 \Omega_H^4$ [10]. Most semi-analytical work on BZ jet powers focus on such extensions of

Ω_H . However, note that this formulation ignores the effect of BH spin on ϕ_H as well as the properties of the accretion flow, which becomes an important assumption for self-consistently evolved accreting BHs. In the magnetically saturated limit (i.e., the MAD limit), the magnetic flux at the event horizon reaches the maximum possible value for a particular disk geometry. Decreasing the geometrical thickness of the accretion flow lowers the corresponding MAD ϕ_H value [31]. Hence, for our models, which are applicable for geometrically-thick, sub-Eddington accretion flows such as M87* ($\dot{M} \ll 10^{-3} \dot{M}_{Edd}$) [32], the time-averaged ϕ_H could be deemed as an upper-limit. We find that ϕ_H depends strongly on not only the BH spin, verifying results from previous work on Kerr BHs [12], but also on each non-Kerr deviation parameter.

In summary, we present the first 3D numerical simulations of spinning non-Kerr BHs, building the most extensive library of 3D GRMHD simulations to date. We demonstrate that the Blandford-Znajek mechanism describes relativistic jet launching for a large class of BHs using a parameterised BH metric. Further, we find that large degeneracies exist in both outflow efficiency as well as shadow and image sizes between Kerr and non-Kerr BHs. Thus, caution should be exercised when inferring the BH spin from current horizon-scale and jet observations. However, even for the non-Kerr models that exhibit shadow size deviations within the measured bounds from M87*, there is a large change in the jet efficiency, which could affect the 86GHz–230GHz spectral index and polarisation signatures especially during flaring events [33, 34]. Therefore, horizon-scale image structures with future high-angular resolution VLBI, together with accurate independent measurements of the BH mass (such as for M87*) and jet power, have the potential to more stringently constrain the space-time properties of supermassive BHs.

ACKNOWLEDGMENTS

KC, PK and RN are supported in part by grants from the Gordon and Betty Moore Foundation and the John Templeton Foundation to the Black Hole Initiative at Harvard University, and by NSF award OISE-1743747. ZY acknowledges support from a UK Research and Innovation (UKRI) Stephen Hawking Fellowship. This research was enabled by support provided by a INCITE program award PHY129, using resources from the Oak Ridge Leadership Computing Facility, Summit, which is a US Department of Energy office of Science User Facility supported under contract DE-AC05-00OR22725, as well as Calcul Quebec (<http://www.calculquebec.ca>) and Compute Canada (<http://www.computeCanada.ca>). This work has made use of NASA's Astrophysics Data System (ADS).

[1] B. R. McNamara and P. E. J. Nulsen, *New Journal of Physics* **14**, 055023 (2012), [arXiv:1204.0006 \[astro-ph.CO\]](https://arxiv.org/abs/1204.0006).
[2] M. A. Bourne and D. Sijacki, *MNRAS* **472**, 4707 (2017), <http://oup.prod.sis.lan/mnras/article-pdf/472/4/4707/21076575/stx2269.pdf>.

[3] S. Cielo, V. Antonuccio-Delogu, J. Silk, and A. D. Romeo, *MNRAS* **467**, 4526 (2017), [arXiv:1701.07825 \[astro-ph.GA\]](https://arxiv.org/abs/1701.07825).
[4] J. Silk and M. J. Rees, *A&A* **331**, L1 (1998), [arXiv:1211.2803 \[astro-ph.HE\]](https://arxiv.org/abs/1211.2803).
[5] J. Magorrian *et al.*, *ApJ* **115**, 2285 (1998).

- [6] A. C. Fabian, *Annual Review of Astronomy and Astrophysics* **50**, 455 (2012), <https://doi.org/10.1146/annurev-astro-081811-125521>.
- [7] C. M. Harrison, T. Costa, C. N. Tadhunter, A. Flütsch, D. Kakkad, M. Perna, and G. Vietri, *Nature Astronomy* **2**, 198 (2018), <https://arxiv.org/abs/1802.10306>.
- [8] R. D. Blandford and R. L. Znajek, *MNRAS* **179**, 433 (1977).
- [9] J. C. McKinney and C. F. Gammie, *ApJ* **611**, 977 (2004), [astro-ph/0404512](https://arxiv.org/abs/astro-ph/0404512).
- [10] A. Tchekhovskoy, R. Narayan, and J. C. McKinney, *ApJ* **711**, 50 (2010), [arXiv:0911.2228](https://arxiv.org/abs/0911.2228).
- [11] A. Tchekhovskoy, J. C. McKinney, and R. Narayan, in *Journal of Physics Conference Series*, Journal of Physics Conference Series, Vol. 372 (2012) p. 012040, [arXiv:1202.2864](https://arxiv.org/abs/1202.2864) [astro-ph.HE].
- [12] R. Narayan, A. Chael, K. Chatterjee, A. Ricarte, and B. Curd, *MNRAS* **511**, 3795 (2022), [arXiv:2108.12380](https://arxiv.org/abs/2108.12380) [astro-ph.HE].
- [13] K. Chatterjee and R. Narayan, *ApJ* **941**, 30 (2022), [arXiv:2210.08045](https://arxiv.org/abs/2210.08045) [astro-ph.HE].
- [14] B. Ripperda, M. Liska, K. Chatterjee, G. Musoke, A. A. Philippov, S. B. Markoff, A. Tchekhovskoy, and Z. Younsi, *ApJL* **924**, L32 (2022), [arXiv:2109.15115](https://arxiv.org/abs/2109.15115) [astro-ph.HE].
- [15] Event Horizon Telescope Collaboration *et al.*, *ApJL* **910**, L13 (2021), [arXiv:2105.01173](https://arxiv.org/abs/2105.01173) [astro-ph.HE].
- [16] Event Horizon Telescope Collaboration *et al.*, *ApJL* **875**, L5 (2019), [arXiv:1906.11242](https://arxiv.org/abs/1906.11242) [astro-ph.GA].
- [17] Event Horizon Telescope Collaboration *et al.*, *ApJL* **930**, L16 (2022).
- [18] T. Johannsen and D. Psaltis, *Phys. Rev. D* **83**, 124015 (2011), [arXiv:1105.3191](https://arxiv.org/abs/1105.3191) [gr-qc].
- [19] T. Johannsen, *Phys. Rev. D* **88**, 044002 (2013), [arXiv:1501.02809](https://arxiv.org/abs/1501.02809) [gr-qc].
- [20] T. Johannsen, *ApJ* **777**, 170 (2013), [arXiv:1501.02814](https://arxiv.org/abs/1501.02814) [astro-ph.HE].
- [21] Z. Younsi, D. Psaltis, and F. Özel, *ApJ* **942**, 47 (2023), [arXiv:2111.01752](https://arxiv.org/abs/2111.01752) [astro-ph.HE].
- [22] K. Akiyama *et al.* (Event Horizon Telescope), *ApJL* **875**, L6 (2019), [arXiv:1906.11243](https://arxiv.org/abs/1906.11243) [astro-ph.GA].
- [23] D. Psaltis *et al.* (Event Horizon Telescope), *PRL* **125**, 141104 (2020), [arXiv:2010.01055](https://arxiv.org/abs/2010.01055) [gr-qc].
- [24] P. Kocherlakota *et al.* (Event Horizon Telescope), *PRD* **103**, 104047 (2021), [arXiv:2105.09343](https://arxiv.org/abs/2105.09343) [gr-qc].
- [25] Z. Younsi, K. Wu, and S. V. Furst, *A&A* **545**, A13 (2012).
- [26] Z. Younsi, O. Porth, Y. Mizuno, C. M. Fromm, and H. Olivares, *arXiv e-prints*, [arXiv:1907.09196](https://arxiv.org/abs/1907.09196) (2019), [arXiv:1907.09196](https://arxiv.org/abs/1907.09196) [astro-ph.HE].
- [27] EHTC, K. Akiyama, A. Alberdi, W. Alef, K. Asada, R. Azulay, A.-K. Baczkó, D. Ball, M. Baloković, J. Barrett, *et al.*, *ApJL* **875**, L5 (2019).
- [28] L. Sironi, M. Petropoulou, and D. Giannios, *MNRAS* **450**, 183 (2015).
- [29] C. M. Fromm, A. Cruz-Orsio, Y. Mizuno, A. Nathanail, Z. Younsi, O. Porth, H. Olivares, J. Davelaar, H. Falcke, M. Kramer, and L. Rezzolla, *A&A* **660**, A107 (2022), [arXiv:2111.02518](https://arxiv.org/abs/2111.02518) [astro-ph.HE].
- [30] K. Tanabe and S. Nagataki, *Phys. Rev. D* **78**, 024004 (2008), [arXiv:0802.0908](https://arxiv.org/abs/0802.0908).
- [31] B. Lowell, J. Jacquemin-Ide, A. Tchekhovskoy, and A. Duncan, *arXiv e-prints*, [arXiv:2302.01351](https://arxiv.org/abs/2302.01351) (2023), [arXiv:2302.01351](https://arxiv.org/abs/2302.01351) [astro-ph.HE].
- [32] K. Chatterjee, A. Chael, P. Tiede, Y. Mizuno, R. Emami, C. Fromm, A. Ricarte, L. Blackburn, F. Roelofs, M. D. Johnson, S. S. Doeleman, P. Arras, A. Fuentes, J. Knollmüller, N. Kossogorov, G. Lindahl, H. Müller, N. Patel, A. Raymond, E. Traianou, and J. Vega, *Galaxies* **11**, 38 (2023), [arXiv:2212.01804](https://arxiv.org/abs/2212.01804) [astro-ph.HE].
- [33] Z. Gelles, K. Chatterjee, M. Johnson, B. Ripperda, and M. Liska, *Galaxies* **10**, 107 (2022), [arXiv:2210.07273](https://arxiv.org/abs/2210.07273) [astro-ph.HE].
- [34] H. Jia, B. Ripperda, E. Quataert, C. J. White, K. Chatterjee, A. Philippov, and M. Liska, *MNRAS* **526**, 2924 (2023), [arXiv:2301.09014](https://arxiv.org/abs/2301.09014) [astro-ph.HE].
- [35] M. T. P. Liska *et al.*, *ApJS* **263**, 26 (2022), [arXiv:1912.10192](https://arxiv.org/abs/1912.10192) [astro-ph.HE].
- [36] M. Liska, C. Hesp, A. Tchekhovskoy, A. Ingram, M. van der Klis, and S. Markoff, *MNRAS* **474**, L81 (2018), [arXiv:1707.06619](https://arxiv.org/abs/1707.06619) [astro-ph.HE].
- [37] K. Chatterjee, M. Liska, A. Tchekhovskoy, and S. B. Markoff, *MNRAS* **490**, 2200 (2019), [arXiv:1904.03243](https://arxiv.org/abs/1904.03243) [astro-ph.HE].
- [38] L. G. Fishbone and V. Moncrief, *ApJ* **207**, 962 (1976).
- [39] S. M. Ressler, A. Tchekhovskoy, E. Quataert, and C. F. Gammie, *MNRAS* **467**, 3604 (2017), [arXiv:1611.09365](https://arxiv.org/abs/1611.09365) [astro-ph.HE].
- [40] Z. Younsi, A. Zhidenko, L. Rezzolla, R. Konoplya, and Y. Mizuno, *Phys. Rev. D* **94**, 084025 (2016), [arXiv:1607.05767](https://arxiv.org/abs/1607.05767) [gr-qc].
- [41] Z. Younsi, O. Porth, Y. Mizuno, C. M. Fromm, and H. Olivares, in *IAU Symposium*, IAU Symposium, Vol. 342, edited by K. Asada, E. de Gouveia Dal Pino, M. Giroletti, H. Nagai, and R. Nemmen (2020) pp. 9–12, [arXiv:1907.09196](https://arxiv.org/abs/1907.09196) [astro-ph.HE].
- [42] M. Mościbrodzka, H. Falcke, and H. Shiokawa, *A&A* **586**, A38 (2016).

Metric	Non-Kerr value	BH spin parameter
Kerr	–	0, ± 0.3 , ± 0.5 , ± 0.7 , ± 0.9 , ± 0.94 , ± 0.998
JP α_{13}	–2	0, ± 0.3 , ± 0.5
JP α_{13}	+2	0, ± 0.3 , ± 0.5 , ± 0.7
JP α_{13}	+6	0, ± 0.3 , ± 0.5 , ± 0.7
JP α_{22}	–2	0, ± 0.3 , ± 0.5 , ± 0.7 , 0.9
JP α_{22}	+2	0, ± 0.3 , ± 0.5 , ± 0.7 , 0.9
JP α_{22}	+5	0, ± 0.3 , ± 0.5 , ± 0.7
JP α_{22}	+8	± 0.3 , ± 0.5
JP ϵ_3	–3	0, ± 0.3 , ± 0.5
JP ϵ_3	+6	0, ± 0.3 , ± 0.5

TABLE I. List of GRMHD simulations performed in this work, together with their respective spin and non-Kerr parameter values.

Appendix A: Numerical Methods

General relativistic magnetohydrodynamics simulations. We use the GPU-accelerated code H-AMR [35] which solves the GRMHD equations in a fixed background spacetime. We assume logarithmic spherical polar in-going Kerr-Schild coordinates $(t, \log r, \theta, \varphi)$ and natural units, i.e. $G = c = 1$, which normalises the gravitational radius $r_g = GM_{\text{BH}}/c^2$ to the BH mass M . Our simulations have an effective grid resolution of $N_r \times N_\theta \times N_\varphi = 348 \times 240 \times 256$. The grid extends from $r/M \in (1.1525, 10000)$, $\theta \in (0, \pi)$ and $\varphi \in (0, 2\pi)$. In order to speed up our simulations, we derefine the φ -resolution by a factor of 4 near the polar axis. We adopt outflowing radial boundary conditions (BCs), transmissive polar BCs and peri-

odic BCs in the φ -direction [35–37]. We initialise the disk in the form of an equilibrium hydrodynamic torus [38] around a BH with a fiducial spin value of $a = 0.9375$. We set up a standard MAD magnetic field configuration [e.g., 13]. For our gas thermodynamics, we assume an ideal gas equation of state with an adiabatic index of 13/9. The initial magnetic field strength is normalised by setting the initial maximum gas-to-magnetic pressure ratio to 100. For tackling the evacuated region in the jet funnel, we adopt the density floor injection scheme of Ressler *et al.* [39] when the magnetisation exceeds 20. Table I provides the list of models used in this work

General relativistic radiative transfer calculations. We use the GRRT raytracing code BHOSS [21, 25, 40, 41]. We assume that the emission mechanism is thermal synchrotron radiation for a (relativistic) Maxwell-Jüttner electron population. The electron temperature is calculated from the temperature of the ions via the ion-to-electron temperature ratio $T_i/T_e := (R_{\text{low}} + \beta^2 R_{\text{high}})/(1 + \beta^2)$ [42], where the local plasma- β parameter, together with the dimensionless parameters R_{low} and R_{high} , control the coupling between ions and electrons. We choose $R_{\text{low}} = 1$ and $R_{\text{high}} = 40$ in all models, consistent with parameter fits of recent polarimetric observations of M87* [15].